Desalination 566 (2023) 116909

Contents lists available at ScienceDirect

Desalination

journal homepage: www.elsevier.com/locate/desal

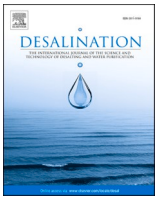

Recovery of ultra-high purity reactive magnesia from reject brine and its comparison with commercial magnesia

Haoliang Dong [a], Xi Xiao [a], En-Hua Yang [a], Cise Unluer [b,*]

[a] School of Civil and Environmental Engineering, Nanyang Technological University, 50 Nanyang Avenue, Singapore
[b] Department of Mechanical, Aerospace and Civil Engineering, University of Manchester, Manchester M13 9PL, United Kingdom

HIGHLIGHTS

- Reactive MgO can be synthesized from desalination reject brine, which is rich in Mg^{2+}.
- Presence of other components (calcium) in reject brine leads to precipitation of other phases with $Mg(OH)_2$.
- This study improved purity and yield of MgO synthesized by selective precipitation under controlled pH.
- Synthesis of magnesium oxalate dihydrate with a high purity (99.6 %) and a magnesium recovery rate (94.1 %) was achieved.
- Reactive MgO with a specific surface area of 30.2 m^2/g was obtained after calcination at 700 °C for 2 h.

ARTICLE INFO

Keywords:
Reject brine
Oxalic acid
Magnesium oxalate
MgO
Selective precipitation

ABSTRACT

CO_2 emissions and energy consumption associated with ordinary Portland cement production have increased the urgency for the development of alternative construction materials. Reactive magnesia cement (RMC) has been widely studied in the recent years due to the lower calcination temperature used during its production and its ability to permanently sequester CO_2. In addition to the calcination of magnesite, reactive MgO, the main component of RMC, can also be synthesized from reject brine, which is rich in Mg^{2+}. However, the presence of other components such as calcium in reject brine leads to the precipitation of other mineral phases together with $Mg(OH)_2$, thereby reducing the purity of the final product. With the goal of improving the purity and yield of MgO synthesized at the end of this process, this study proposed a selective precipitation approach under a controlled pH. An optimum condition was determined for the synthesis of magnesium oxalate dihydrate with an ultra-high purity of 99.6 % and a high magnesium recovery rate of 94.1 %. Reactive MgO with a specific surface area of 30.2 m^2/g was obtained after the calcination of the synthesized magnesium oxalate dihydrate at 700 °C for 2 h, which was higher than some of the commercially available MgO powders.

1. Introduction

The increased concentration of carbon dioxide (CO_2) in the atmosphere is a major contributor to climate change. Every year, the production of cement is estimated to account for 7 % global anthropogenic CO_2 emissions [1]. As the most extensively used man-made material in the world, the annual production of Portland cement (PC) exceeds 4 billion tons [2]. The production of cement is an energy intensive process accompanied with a significant CO_2 release, which involves burning fossil fuels to achieve ultra-high temperatures of up to 1450–1550 °C for the calcination of limestone ($CaCO_3$) [3]. It is reported that the production of 1 ton of cement consumes an average of 4 GJ of energy [4] and releases an 0.8 tons of CO_2 [5]. To mitigate the energy consumption and carbon footprint of the cement industry, recent research initiatives have been directed towards identifying alternative binders for ordinary PC.

One potential binder system involves the use of reactive magnesia cement (RMC), whose main component is reactive magnesia (MgO) [6,7]. The main MgO production is through the calcination of magnesite ($MgCO_3$, Eq. (1), dry route). Compared to PC, the production of MgO via the decomposition of magnesite takes place at lower temperatures of 700–900 °C [8,9]. Besides the dry route, reactive MgO can also be synthesized via the wet route, which relies on the extraction of MgO from Mg-rich sources such as seawater or brine [10], as shown in Eqs.

* Corresponding author.
E-mail address: cise.unluer@manchester.ac.uk (C. Unluer).

https://doi.org/10.1016/j.desal.2023.116909
Received 29 June 2023; Received in revised form 7 August 2023; Accepted 8 August 2023
Available online 9 August 2023
0011-9164/© 2023 The Authors. Published by Elsevier B.V. This is an open access article under the CC BY license (http://creativecommons.org/licenses/by/4.0/).

(2) and (3). As a part of this approach, Mg^{2+} is first precipitated from these Mg-rich sources in the form of $Mg(OH)_2$ through the addition of a base such as lime (CaO), dolime (CaO·MgO), ammonia solution (NH_4OH) and sodium hydroxide (NaOH) [10–12]. This is then followed by the calcination of $Mg(OH)_2$ to produce MgO. The chemical reactions involved in the synthesis of MgO from the wet route do not release extra CO_2. When compared to the dry route, reactive MgO synthesized via the wet route often possesses higher purity and reactivity [13], which could enable its use as an additive or catalyst in high value added applications within the pharmaceutical and semiconductor industries [14,15]. In addition to this alternative production routes, another advantage of the RMC system is the strength gain mechanism, which mainly relies on carbonation, therefore enabling the permanent sequestration of CO_2 in the form of stable carbonates [16].

$$MgCO_3 \overset{\text{Calcination}}{\rightarrow} MgO + CO_2 \quad (1)$$

$$CaO/CaO{\cdot}MgO + H_2O + MgCl_2 \rightarrow Mg(OH)_2 + CaCl_2 \quad (2)$$

$$Mg(OH)_2 \overset{\text{Calcination}}{\rightarrow} MgO + H_2O \quad (3)$$

Singapore is considered to be one of the most water-stressed countries in the world due to the lack of natural water resources and limited land space for water storage. In line with its geographical location, Singapore is surrounded by seawater, which provides this island country a solution to freshwater shortage by seawater desalination. With five desalination plants, 30 % of drinking water in Singapore (i.e. 190 million gallons or 852,150 m^3 per day) is provided via desalination. It is reported that the production of 1 m^3 of desalinated water generates an equal amount of reject brine [17]. Typically, reject brine, which has a high salinity and large amounts of dissolved chemicals, is discharged directly back to the sea, posing a harm for the local marine life and water quality [18,19].

Previous studies reported that valuable resources such as salts, metals and chemicals could be recovered from seawater or reject brine. Compared with seawater, desalination brine has a 1.5–2 times higher salinity after the widely adopted reverse osmosis (SWRO) treatment applied to seawater [20]. Researchers are therefore looking into extracting critical and strategic materials from reject brine, one of the key ones being magnesium. In recent years, significant resources and funding have been allocated both in Europe and North America to extract minerals directly from seawater or brine. Some of these initiatives include the EU-funded ZERO BRINE (€1.1 billion) and SEArcularMINE (€5.8 million) projects focusing on extracting minerals from brine (e.g. magnesium, lithium, and other trace elements) [21,22]. Recently, the U.S. Department of Energy has added magnesium to its list of critical materials for domestic production. In response to this, the Pacific Northwest National Laboratory (PNNL) and the University of Washington (UW) collaborated to develop a cutting-edge laminar coflow method to isolate pure magnesium salt from seawater [23].

Magnesium has a variety of potential uses in clean energy technologies, including carbon capture, low-carbon cements and next-generation batteries. In the context of significant global sustainability efforts, the concentrated presence of Mg^{2+} in reject brine is an appealing source for MgO recovery. While the recovery of magnesium from brine has been widely studied, recent initiatives involving magnesium extraction focus on the further improvement of extraction efficiency and precise control by exploiting laminar coflow method (LCM) and some selective precipitation technologies (e.g. selective membranes, pH control, selective adsorbents) [21,24–26]. In summary, the recovery of reactive MgO from reject brine presents a promising route for the production of an alternative cementitious binder from waste materials.

In line with the chemical composition of reject brine, in addition to the precipitation of $Mg(OH)_2$, the presence of Ca^{2+} and HCO_3^- in the brine can lead to the co-precipitation of calcium-based compounds (e.g. $CaCO_3$ and $Ca(OH)_2$), which reduces the purity and reactivity of the resulting reactive MgO. The solubility product constant (K_{sp}) for the Mg and Ca-based precipitates at 25 °C are listed in the following Table 1, along with the pH when the crystals start to precipitate, calculated according to the K_{sp}. Earlier studies involving the use of NH_4OH and NaOH for the precipitation of $Mg(OH)_2$ showed that the use of NaOH can result in 6.3–10.8 % calcite co-precipitation at Mg^{2+}:NaOH ratios varying between 1:2 and 1:4 [10]. Another study reported that the use of NH_4OH led to 2–24.4 % calcite co-precipitation when the NH_4OH:reject brine ratio varied between 2.24:200 and 19.08:200 [27].

To avoid the co-precipitation of calcium, Tran et al. [28] proposed the synthesis of magnesium oxalate ($MgC_2O_4{\cdot}2H_2O$) precursor from Salar de Uyuni brine via the addition of oxalic acid. Selective precipitation of calcium oxalate ($CaC_2O_4{\cdot}H_2O$) and $MgC_2O_4{\cdot}2H_2O$ can be achieved via a proper control of pH. Accordingly, $CaC_2O_4{\cdot}H_2O$ first precipitated at pH < 1 and removed from the brine (Eq. (4)) and followed by Mg^{2+} precipitation in the form of $MgC_2O_4{\cdot}2H_2O$ at pH > 1 (Eq. (5)). The yielded $MgC_2O_4{\cdot}2H_2O$ had an ultra-high purity of up to 99.5 %. Afterwards, a further calcination step was applied to thermally decompose $MgC_2O_4{\cdot}2H_2O$ and produce reactive MgO, as shown in Eq. (6). Although the study has demonstrated the feasibility of the selective precipitation, the optimal calcination temperature and duration were not investigated, and the properties of the obtained MgO products were not characterized. Therefore, in this study, various calcination temperatures (700–900 °C) and calcination durations (2−12h) were incorporated in the production of reactive MgO, whose properties were further investigated to analyze its suitability for different applications.

$$Ca^{2+} + H_2C_2O_4{\cdot}2H_2O \rightarrow CaC_2O_4{\cdot}H_2O \ (pH \leq 1) \quad (4)$$

$$Mg^{2+} + H_2C_2O_4{\cdot}2H_2O \rightarrow MgC_2O_4{\cdot}2H_2O \ (pH > 1) \quad (5)$$

$$MgC_2O_4{\cdot}2H_2O \overset{\text{Calcination}}{\rightarrow} MgO + 2H_2O + CO + CO_2 \quad (6)$$

To achieve these goals, the selective precipitation of Ca^{2+} and Mg^{2+} from Singapore local reject brine via the addition of oxalic acid ($H_2C_2O_4{\cdot}2H_2O$), followed by the production of ultra-high purity reactive MgO, were demonstrated. A systematic investigation was carried out to reveal key factors governing the yield and properties of magnesium oxalate precipitates and determined the optimum conditions for the synthesis of $MgC_2O_4{\cdot}2H_2O$ with a high purity and yield from reject brine. The resulting $MgC_2O_4{\cdot}2H_2O$ was then calcined to produce high-purity reactive MgO. The influence of calcination temperature and duration on the specific surface area (SSA), crystallite size, primary particle size and pore volume of the obtained MgO was presented after a comprehensive investigation. Finally, a comparison of the reactive MgO produced via this route with commercial counterparts was provided.

2. Materials and methodology

2.1. Chemical composition of reject brine

Differing from seawater and natural brine, a large number of suspended solids was presented in reject brine, which had to be first removed and filtered through a 45 μm membrane before any further experiments and analysis. The chemical composition of reject brine used in the current study was analyzed by inductively coupled plasma optical emission spectrometry (ICP-OES, PerkinElmer Optima DV2000) and ion chromatography (IC). Before the test, the equipment was calibrated to ensure accuracy. As shown in Table 2, Cl^-, Na^+, SO_4^{2-}, Mg^{2+}, K^+ and

Table 1
K_{sp} and precipitation pH of Mg and Ca-based phases in the reject brine.

Chemical phase	K_{sp}	Precipitation pH
$Mg(OH)_2$	1.5×10^{-11}	10.38
$Ca(OH)_2$	7.9×10^{-6}	12.12
$CaCO_3$	3.8×10^{-9}	10.59

Table 2
Chemical composition of reject brine used in the current study.

Component	Cl^-	Na^+	SO_4^{2-}	Mg^{2+}	K^+	Ca^{2+}	Sr^{2+}	B^{3+}	Si^{4+}	Li^+
ppm	84,615 ± 87.2	20,800 ± 42.5	5576 ± 9.6	2166 ± 4.9	1043 ± 4.8	727 ± 4.2	6.8 ± 0.1	5.8 ± 0.1	0.6 ± 0.1	0.5 ± 0.1

Ca^{2+} were the most abundant components in reject brine.

2.2. Selective precipitation of $MgC_2O_4{\cdot}2H_2O$ from reject brine

Reject brine was obtained from Tuaspring desalination plant, which is a local desalination plant in Singapore. The plant is the largest desalination plant in South East Asia, producing 318,500 m^3 of desalinated water per day via reverse osmosis technology. Analytical grade oxalic acid ($H_2C_2O_4{\cdot}2H_2O$) and sodium hydroxide (NaOH) were sourced from Sigma-Aldrich and VWR Singapore Pte. Ltd., respectively.

Previous studies [28,29] show that $CaC_2O_4{\cdot}H_2O$ precipitates through the reaction of Ca^{2+} and $H_2C_2O_4{\cdot}2H_2O$ at pH $\leq$ 1 (Eq. (4)) while the reaction of Mg^{2+} and $H_2C_2O_4{\cdot}2H_2O$ prevails at pH $>$ 1 to form $MgC_2O_4{\cdot}2H_2O$ precipitates (Eq. (5)) [29,30]. Accordingly, a two-step selective precipitation was adopted in this study. Firstly, crystalline $H_2C_2O_4{\cdot}2H_2O$ was added into 600 ml reject brine under a constant pH of 1 to encourage the precipitation of $CaC_2O_4{\cdot}H_2O$. Two different Ca^{2+}:$H_2C_2O_4{\cdot}2H_2O$ molar ratios of 1:1 and 1:2 were used to study the effects of the Ca^{2+}:$H_2C_2O_4{\cdot}2H_2O$ ratio on the yield and properties of $CaC_2O_4{\cdot}H_2O$ precipitates. The lower bound of the molar ratio was determined based on Eq. (4). Theoretically, the synthesis of 1 mol $CaC_2O_4{\cdot}H_2O$ requires the reaction of 1 mol Ca^{2+} with 1 mol oxalic acid. Thus, a molar ratio of 1:1 was used as the lower bound. An upper bound of molar ratio of 1:2 was selected to ensure high removal rate of Ca^{2+} in the reject brine. During the reaction, NaOH was continuously added to control and maintain the pH of the solution at the designed value of 1. In addition, the solution was stirred constantly at 200 rpm with a magnetic stirrer in a controlled laboratory environment (1 atm, 25 °C). The pH and the temperature of the solution were continuously monitored by a Mettler Toledo pH/Ion meter S220 pH/thermometer. Before each experiment, the pH meter was calibrated with three standard reference solutions with pH of 4, 7 and 10, respectively. After the reaction, centrifugation was adopted to separate the precipitates from the solution. In order to remove the surface-attached ions, the collected solid precipitates were washed three times with ultra-pure water. Then the washed solids were oven-dried for 24 h at 105 °C before grinding into powder form for further analysis.

Following the first step after the removal of the solid precipitates, additional $H_2C_2O_4{\cdot}2H_2O$ was added into the residue reject brine. Three molar ratios of Mg^{2+}:$H_2C_2O_4{\cdot}2H_2O$ (i.e. 1:1, 1:1.25 and 1:1.5) and two pH values (i.e. 2 and 3) were studied to reveal the effects of Mg^{2+}:$H_2C_2O_4{\cdot}2H_2O$ ratio and pH on the yield and properties of $MgC_2O_4{\cdot}2H_2O$ precipitates. The lower bound of the molar ratio was determined based on Eq. (5). Theoretically, the synthesis of 1 mol $MgC_2O_4{\cdot}2H_2O$ requires the reaction of 1 mol Mg^{2+} with 1 mol oxalic acid. Thus, a molar ratio of 1:1 was used as the lower bound. An upper bound of molar ratio of 1:1.5 was determined after initial trials as Mg^{2+} can be recovered 100 % at this ratio. The reaction conditions, monitoring scheme and collection of precipitates were similar to those used in step 1. To maintain a predetermined pH value in the solution, NaOH was used as a pH controller, as the addition of oxalic acid significantly lowered the pH of the solution to below 1. Moreover, the reaction between Mg^{2+} and oxalic acid caused constant fluctuations of the solution pH. As the yield and chemical reaction can be affected by the pH level, in order to investigate the influence of the solution pH on the yield and purity of the precipitates, it is essential to maintain a constant pH during the reaction. Therefore, NaOH was employed as a pH adjuster to regulate and maintain the solution pH.

2.3. Production and characterization of reactive MgO from $MgC_2O_4{\cdot}2H_2O$

To investigate the Ca^{2+} and Mg^{2+} recovery efficiency after each step of precipitation, the Ca^{2+} and Mg^{2+} ion concentration in the reject brine was measured after each precipitation step was completed through inductively coupled plasma optical emission spectrometry (ICP-OES, PerkinElmer Optima DV2000). To study the crystal structures of solid precipitates collected from both step 1 and step 2, x-ray powder diffraction (XRD) was run on a Bruker D8 Advance with a Cu Kα source operated at 40 kV and 40 mA. The wavelength of the emitting radiation was 1.5405 Å and the scan rate was controlled at 0.02°/step with a 2θ range of 5–70°. The thermal property of the precipitates was examined through the thermogravimetric and differential thermal analysis (TG/DTA Pyris Diamond TGA 4000). The operation condition was controlled with a heating rate of 10 °C/min under N_2 flow.

Afterwards, the $MgC_2O_4{\cdot}2H_2O$ precipitates collected at the end of selective precipitation step 2 were further grounded and then calcined at various temperatures (i.e. 700, 800, 900 °C) and for different residence durations (i.e. 2, 6, 12 h) to produce reactive MgO (Eq. (6)). The objective was to investigate the effects of calcination temperature and duration on the properties of reactive MgO.

To study the crystal structures of the obtained MgO, XRD was run with the same configurations as described above. The SSA of the obtained MgO was calculated via the Brunauer-Emmett-Teller (BET) method. The pore volume was tested through the Barrett-Joynet-Halenda (BJH) method, which was captured via the nitrogen adsorption-desorption isotherms. The crystallite size of MgO can be calculated in accordance with the Debye-Scherrer formula (Eq. (7)).

$$G_{XRD} = K{\cdot}\lambda/(\beta{\cdot}cos(\theta)) \quad (7)$$

where λ is the wavelength of the Cu Kα source (λ = 1.5405 Å), β is the line broadening at half the maximum intensity (FWHM) after subtracting the instrumental line broadening, θ is the Bragg angle, and K is the dimensionless shape factor with a typical value of 0.9 [31]. Accordingly, the agglomeration ratio (AR) can be calculated according to Eqs. (8) and (9).

$$\text{Agglomeration ratio (AR)} = G_{BET}/G_{XRD} \quad (8)$$

$$G_{BET} = F/\rho S \quad (9)$$

where G_{BET} is the primary particle size, G_{XRD} is the crystallite size, F is particle-shape factor (6), S is SSA (m^2/g), and ρ is the theoretical density of MgO (3.595 g/cm^3) [32].

3. Results and discussion

3.1. Characterization of $MgC_2O_4{\cdot}2H_2O$

3.1.1. Inductively coupled plasma optical emission spectrometry

Tables 3 and 4 summarize the concentrations of Ca^{2+} and Mg^{2+} in the residual brine and respective recovery efficiency in percentage after the sequential precipitation of $CaC_2O_4{\cdot}H_2O$ and $MgC_2O_4{\cdot}2H_2O$ in steps 1 and 2. In the first step, the recovery percentage was calculated based on the original ion concentration in the brine, as shown in Eq. (10). In the second step, since Ca/Mg ions were partially extracted in step 1, the recovery percentage was calculated based on the residue ion concentration after step 1, as shown in Eq. (11).

Table 3
Concentrations of Ca^{2+} and Mg^{2+} in the residual brine when the initial Ca^{2+}/$H_2C_2O_4{\cdot}2H_2O$ = 1:1.

			Ca^{2+} (ppm)	Recovery (%)	Mg^{2+} (ppm)	Recovery (%)
Step 1 Ca^{2+}:$H_2C_2O_4{\cdot}2H_2O$ = 1:1 (pH = 1)			30.6 ± 2.9	95.8	1900.7 ± 21.7	12.2
Step 2	Mg^{2+}: $H_2C_2O_4{\cdot}2H_2O$ = 1:1	pH = 2	13.1 ± 1.1	57.2	829.9 ± 41.3	56.3
		pH = 3	0	100	452.4 ± 21.7	76.2
	Mg^{2+}: $H_2C_2O_4{\cdot}2H_2O$ = 1:1.25	pH = 2	10.1 ± 0.7	67.0	655.0 ± 24.5	65.5
		pH = 3	0	100	334.5 ± 10.4	82.4
	Mg^{2+}: $H_2C_2O_4{\cdot}2H_2O$ = 1:1.5	pH = 2	13.1 ± 0. 5	57.2	605.2 ± 15.7	68.2
		pH = 3	0	100	152.1 ± 9.7	92.0

Table 4
Concentrations of Ca^{2+} and Mg^{2+} in the residual brine when the initial Ca^{2+}/$H_2C_2O_4{\cdot}2H_2O$ = 1:2.

			Ca^{2+} (ppm)	Recovery (%)	Mg^{2+} (ppm)	Recovery (%)
Step 1 Ca^{2+}:$H_2C_2O_4{\cdot}2H_2O$ = 1:2 (pH = 1)			6.3 ± 0.9	99.1	1893.3 ± 7.4	12.6
Step 2	Mg^{2+}: $H_2C_2O_4{\cdot}2H_2O$ = 1:1	pH = 2	1.2 ± 0.5	81.0	704.1 ± 30.4	62.8
		pH = 3	0	100	149.5 ± 7.9	92.1
	Mg^{2+}: $H_2C_2O_4{\cdot}2H_2O$ = 1:1.25	pH = 2	0	100	666.2 ± 25.7	64.8
		pH = 3	0	100	125.3 ± 13.4	93.4
	Mg^{2+}: $H_2C_2O_4{\cdot}2H_2O$ = 1:1.5	pH = 2	0	100	624 ± 20.6	67.0
		pH = 3	0	100	110.9 ± 4.9	94.1

$$\text{Recovery of step 1} = 100\% - \frac{\text{Residue ion concentration after step 1}}{\text{Original ion concentration in reject brine}} \times 100\% \quad (10)$$

$$\text{Recovery of step 2} = 100\% - \frac{\text{Residue ion concentration after step 2}}{\text{Residue ion concentration after step 1}} \times 100\% \quad (11)$$

As can be seen from Table 3, 96 % of Ca^{2+} was recovered while 12 % of Mg^{2+} was co-precipitated in the first step precipitation at a molar ratio of Ca^{2+}:$H_2C_2O_4{\cdot}2H_2O$ = 1:1 (pH = 1). When Ca^{2+}:$H_2C_2O_4{\cdot}2H_2O$ molar ratio increased to 1:2 (pH = 1), higher Ca^{2+} and Mg^{2+} recovery was obtained (Table 3). In the second step precipitation, pH was the dominant factor to control the Mg^{2+} recovery. According to Table 3, by increasing Mg^{2+}:$H_2C_2O_4{\cdot}2H_2O$ ratio from 1:1 to 1:1.5 while fixing pH = 2 or pH = 3, the Mg^{2+} recovery increased around 20 %. Differently, by increasing the pH from 2 to 3 while fixing other parameters, the recovery of Mg^{2+} can increase >46 %. For example, in Table 4, while fixing Mg^{2+}:$H_2C_2O_4{\cdot}2H_2O$ = 1:1.5, the increase of pH from 2 to 3 has led to the increase of Mg^{2+} recovery efficiency from 67 % to 94.1 %. According to the two tables, the highest Mg^{2+} recovery was 94.1 %, which was obtained under a Ca^{2+}:$H_2C_2O_4{\cdot}2H_2O$ molar ratio of 1:2 at pH of 1 for the first step precipitation to remove Ca^{2+}, and a Mg^{2+}:$H_2C_2O_4{\cdot}2H_2O$ molar ratio of 1:1.5 at pH of 3 for the second step precipitation. Afterwards, the high yield and high purity magnesium oxalate obtained from this optimum condition was used for further thermal analysis and calcination to produce reactive MgO under different conditions.

3.1.2. XRD of solid precipitates obtained in selective precipitate process

The XRD diffractograms of solids precipitated under different Ca^{2+}:$H_2C_2O_4{\cdot}2H_2O$ and Mg^{2+}:$H_2C_2O_4{\cdot}2H_2O$ molar ratios and pH are illustrated in Fig. 1. In the first step, when Ca^{2+} was recovered through precipitation at pH = 1, Fig. 1(a)-(f) all showed similar patterns, where $CaC_2O_4{\cdot}H_2O$ dominated, along with minor $MgC_2O_4{\cdot}2H_2O$ peaks. The major peaks of $CaC_2O_4{\cdot}H_2O$ were in line with the findings of a previous study [33], where $CaC_2O_4{\cdot}H_2O$ was studied (ICSD 30–782). Comparing Fig. 1(a) with Fig. 1(d), Fig. 1(b) with Fig. 1(d), and Fig. 1(c) with Fig. 1(f), it was observed that, when the ratio of Mg^{2+}:$H_2C_2O_4{\cdot}2H_2O$ was fixed, the intensity of the $MgC_2O_4{\cdot}2H_2O$ peaks increased when Ca^{2+}:$H_2C_2O_4{\cdot}2H_2O$ ratio changed from 1:1 to 1:2, possibly indicating an increased amount of $MgC_2O_4{\cdot}2H_2O$ in the precipitates. Afterwards, in the second step where Mg^{2+} recovered through precipitation as $MgC_2O_4{\cdot}2H_2O$, only $MgC_2O_4{\cdot}2H_2O$ without any $CaC_2O_4{\cdot}H_2O$ or other phases were observed in the XRD diffractograms of precipitates, regardless of the pH and Mg^{2+}:$H_2C_2O_4{\cdot}2H_2O$ ratio. The peaks of $MgC_2O_4{\cdot}2H_2O$ were in line with earlier study [28], where $MgC_2O_4{\cdot}2H_2O$ was synthesized. Overall, the results indicated the effective removal of Ca^{2+} in the first step.

3.1.3. Thermogravimetric and differential thermal analysis

$MgC_2O_4{\cdot}2H_2O$ precipitates obtained from the optimum condition (i.e., first step Ca^{2+}:$H_2C_2O_4{\cdot}2H_2O$ = 1:2 at pH =1, second step Mg^{2+}:$H_2C_2O_4{\cdot}2H_2O$ = 1:1.5 at pH = 3) were characterized by means of the TG/DTA (Fig. 2). As can be seen, two strong peaks associated with two decomposition steps were observed in the DTA curve. The first peak occurred at around 200 °C, which corresponded to the dehydration of $MgC_2O_4{\cdot}2H_2O$, resulting in a mass loss of 24.2 % from 30 °C to 350 °C. The decomposition is shown in Eq. (12), and the mass loss due to water loss is indicated on Fig. 2.

$$MgC_2O_4{\cdot}2H_2O \rightarrow MgC_2O_4 + 2H_2O \quad (12)$$

The second mass loss occurred between 382.3 °C and 552.1 °C as MgC_2O_4 decomposed to MgO due to the liberation of CO and CO_2. From 350 °C to 900 °C, the mass loss due to the decomposition of MgC_2O_4 was accumulated to 48.6 %. The decomposition of MgC_2O_4 is presented in Eqs. (13)–(15), and the resulted mass loss is indicated on Fig. 2.

$$MgC_2O_4 \rightarrow MgCO_3 + CO \quad (13)$$

$$CO + 1/2O_2 \rightarrow CO_2 \quad (14)$$

$$MgCO_3 \rightarrow MgO + CO_2 \quad (15)$$

The mass losses in the two steps measured from the TGA were in good agreement with the theoretical mass loss values due to the dehydration (24.2 %) and decarbonation (48.6 %) of $MgC_2O_4{\cdot}2H_2O$. The residues after TGA (i.e. MgO) had a mass of 27.5 % of the initial sample. Based on Eq. (12), the purity of the synthesized $MgC_2O_4{\cdot}2H_2O$ can be calculated according to Eq. (16), where $M_{MgC2O4{\cdot}2H2O}$ was the molecular weight of $MgC_2O_4{\cdot}2H_2O$ (148.4) and M_{H2O} was the molecular weight of H_2O (18.0). According to the results, the purity of the synthesized $MgC_2O_4{\cdot}2H_2O$ was estimated to be 99.6 %, which was comparable to the findings of previous studies [28].

$$\text{Purity} = 24.2\% \times \frac{M_{MgC2O4{\cdot}2H2O}}{2 \times M_{H2O}} \quad (16)$$

3.2. Characterization of MgO

3.2.1. Microstructure

MgO was obtained from the calcination of $MgC_2O_4{\cdot}2H_2O$ (i.e., synthesized under the optimum condition), at different calcination temperatures and durations. Fig. 3 shows a representative micrograph revealing the morphology of the resulting MgO obtained under different calcination conditions. A profound change in the morphology of MgO

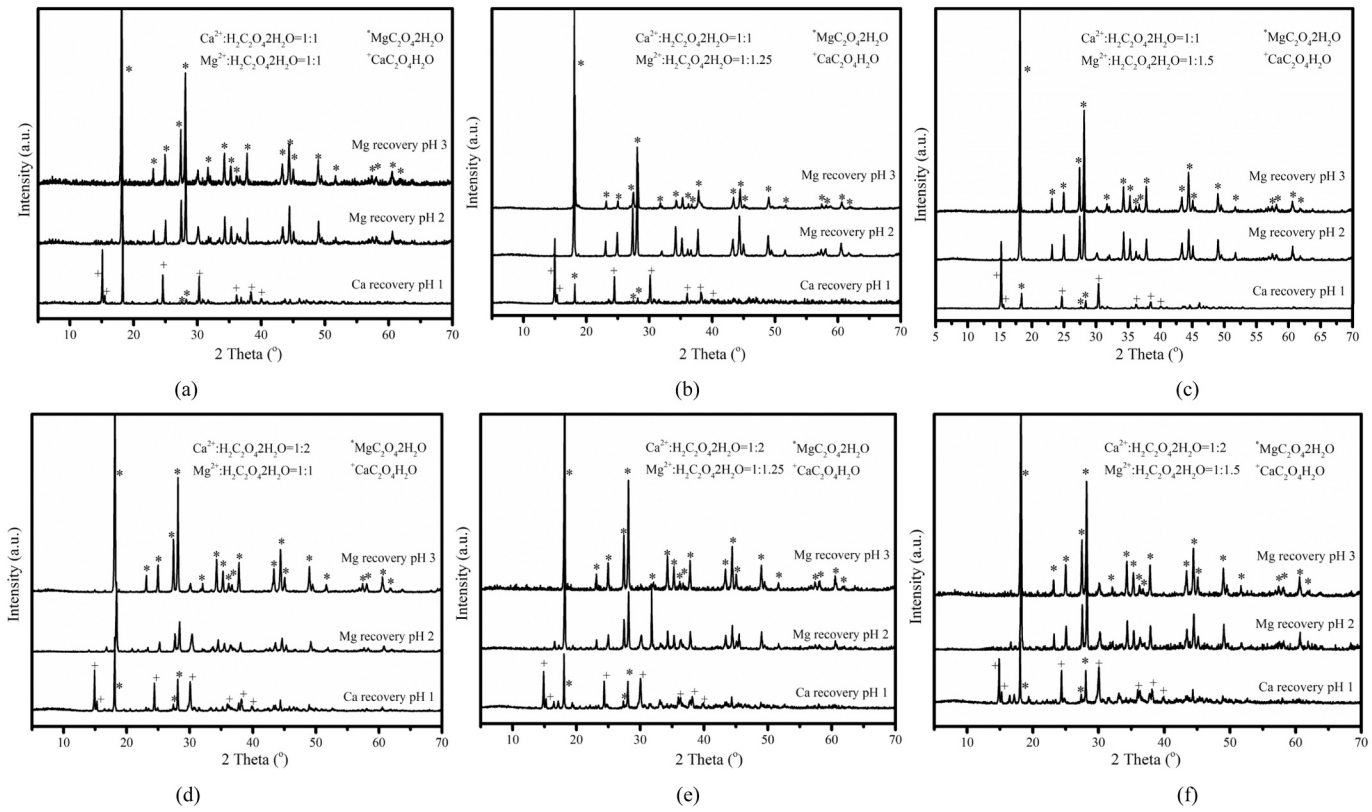

Fig. 1. XRD diffractograms of precipitates synthesized from reject brine with the addition of $H_2C_2O_4{\cdot}2H_2O$ in a two-step reaction process: (a) Ca^{2+}:$H_2C_2O_4{\cdot}2H_2$ = 1:1, Mg^{2+}:$H_2C_2O_4{\cdot}2H_2O$ = 1:1, (b) Ca^{2+}:$H_2C_2O_4{\cdot}2H_2$ = 1:1, Mg^{2+}:$H_2C_2O_4{\cdot}2H_2O$ = 1:1.25, (c) Ca^{2+}:$H_2C_2O_4{\cdot}2H_2$ = 1:1, Mg^{2+}:$H_2C_2O_4{\cdot}2H_2O$ = 1:5, (d) Ca^{2+}:$H_2C_2O_4{\cdot}2H_2$ = 1:2, Mg^{2+}:$H_2C_2O_4{\cdot}2H_2O$ = 1:1, (e) Ca^{2+}:$H_2C_2O_4{\cdot}2H_2$ = 1:2, Mg^{2+}:$H_2C_2O_4{\cdot}2H_2O$ = 1: 1.25, (f) Ca^{2+}:$H_2C_2O_4{\cdot}2H_2$ = 1:2, Mg^{2+}:$H_2C_2O_4{\cdot}2H_2O$ = 1:1.5.

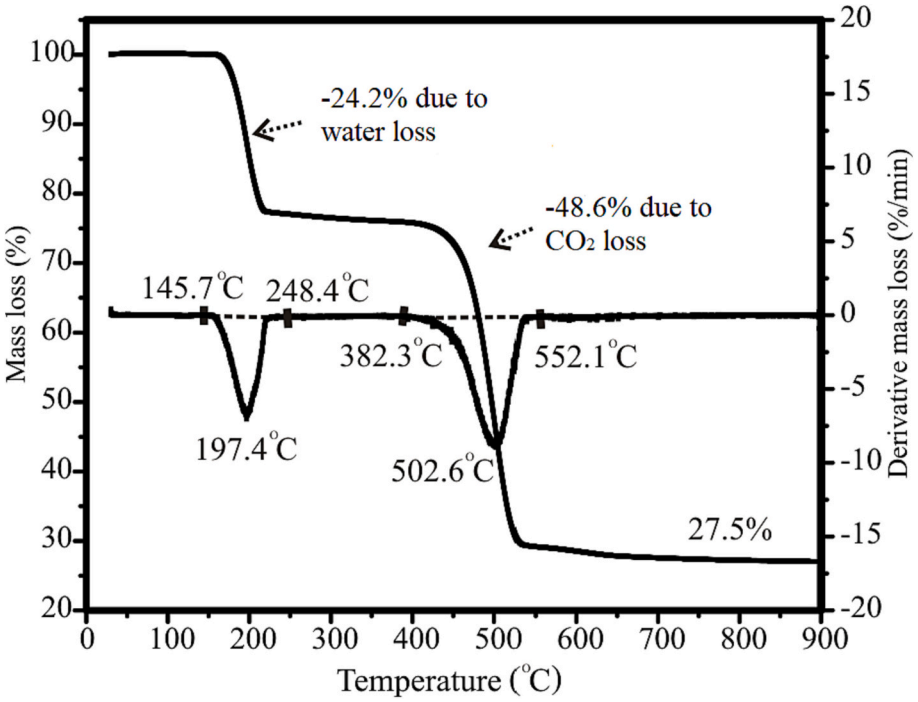

Fig. 2. TG/DTA curve of $MgC_2O_4{\cdot}2H_2O$ synthesized from reject brine (first step Ca^{2+}:$H_2C_2O_4{\cdot}2H_2O$ = 1:2 at pH = 1, and second step Mg^{2+}:$H_2C_2O_4{\cdot}2H_2O$ = 1:1.5 at pH = 3).

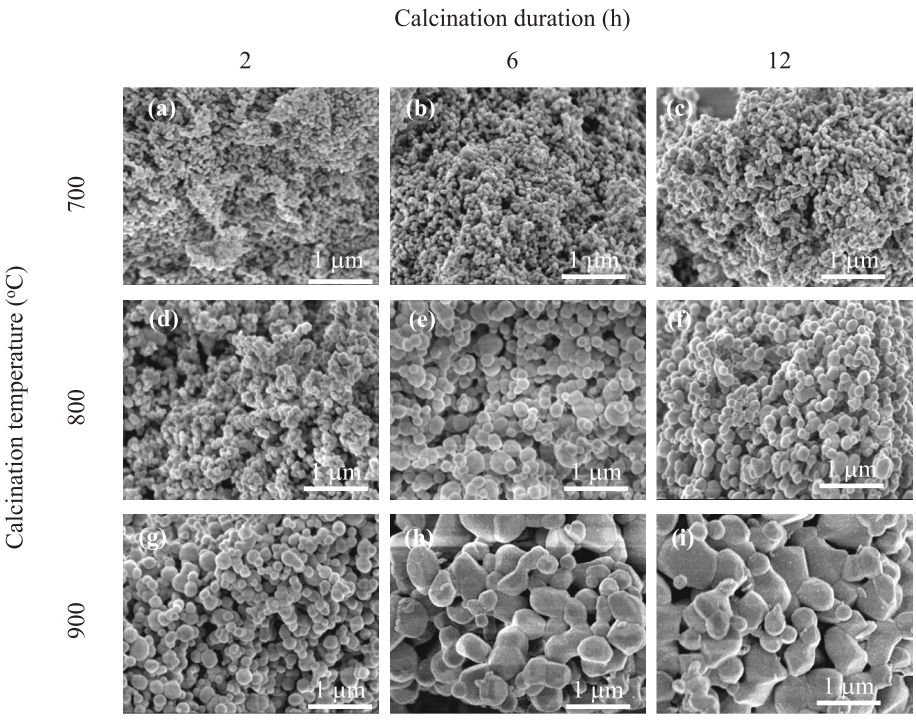

Fig. 3. FESEM images of MgO obtained from calcination of synthesized $MgC_2O_4{\cdot}2H_2O$ (from reject brine) under different calcination temperature and duration.

particles under different calcination conditions was observed. As can be seen, MgO particles generally had round shapes, with a strong tendency to form flocculates. The particle size of MgO increased with increasing calcination temperature and/or duration. The MgO particles tended to form agglomerates (i.e., particles were loosely attached to each other at their edges or corners) at lower calcination temperatures and durations, while they inclined to form aggregates (i.e., particles were rigidly joined together by partial fusion, sintering or growing together) at higher calcination temperatures and durations. This was because dehydration and decarbonation of magnesium oxalate released H_2O, and CO and CO_2, respectively, thereby producing MgO with a loose microstructure. Increased calcination temperature and prolonged calcination duration led to the sintering of MgO, and thus the formation of larger aggregates [34]. To further investigate the relationship between the particle size of MgO and the calcination temperature/duration, a particle size distribution analysis could be implemented.

3.2.2. Textural properties

Fig. 4 presents the SSA of the resulting MgO obtained from calcination of synthesized $MgC_2O_4{\cdot}2H_2O$ (from reject brine) under different calcination temperature and duration. In the current study, the highest SSA of 30.2 m^2/g was obtained when $MgC_2O_4{\cdot}2H_2O$ was calcined at 700 °C for 2 h. Further increases of calcination temperature and/or duration resulted in reduced SSA of MgO due to increased particle size as shown in Fig. 4 above. These findings were in line with those reported in the previous studies [34–39], where MgO properties were directly influenced by the calcination conditions.

3.2.3. Crystallite size, primary particle size and pore volume

Fig. 5 shows XRD patterns of the resulting MgO obtained from the calcination of synthesized $MgC_2O_4{\cdot}2H_2O$ (from reject brine) at different temperatures and durations. The XRD curves exhibited a high degree of similarity. The three distinct peaks observed at 37.0°, 43.0°, and 62.5° (2θ) in the XRD patterns corresponded to the characteristic peaks of MgO as per JCPDS card no. 89–7746. The absence of any other peaks in the XRD diffractograms indicated that the MgO synthesized in the current study had a high purity.

Among the three peaks, the major characteristic peak of MgO at 43.0° (2θ) in the XRD diffractograms (Fig. 5) was used to calculate the crystallite size of MgO (i.e. G_{XRD}). Along with G_{XRD}, the SSA, G_{BET}, agglomeration ratio (AR) and pore volume of MgO were measured and calculated. As can be seen in Table 5, crystallite sizes of MgO increased from 14 to 28 nm when the calcination temperature and duration increased from 700 °C/2 h to 900 °C/12 h. The primary particle size (G_{BET}) of MgO was in the range of 52–170 nm and increased with increasing calcination temperature and duration. The agglomeration ratio (G_{BET}/G_{XRD}) of the resulting MgO increased while the corresponding pore volume decreased with increasing calcination temperature and duration. This may be attributed to the expansion of MgO grains and the primary particles' spontaneous coagulation at higher calcination temperature and duration [40], resulting in higher agglomeration ratios and lower pore volumes which led to lower SSA values as shown in Fig. 4. Furthermore, calcination temperature appeared to have more profound effects on the change of these characteristics than calcination duration.

3.3. Comparison of synthesized MgO with commercial MgO

The characterization results outlined in Table 4 revealed that the optimal calcination conditions for the production of MgO involved heating at 700 °C for 2 h, which yielded the most reactive MgO with a SSA of up to 30.2 m^2/g. These results were then compared to 21 commercially available reactive MgO products, as presented in the literature [39,41]. Together with the reactive MgO obtained in the study, these commercial MgO products were ranked according to their SSA data, as shown in Table 6. Further information on the primary particle size G_{BET}, crystallite size G_{XRD} and agglomeration ratio (AR) of each MgO product were also listed in Table 6.
[1]

The ranking clearly shows that the MgO obtained in this study

[1] SSA = specific surface area; G_{BET} = primary particle size; G_{XRD} = crystallite size; AR = agglomeration ratio

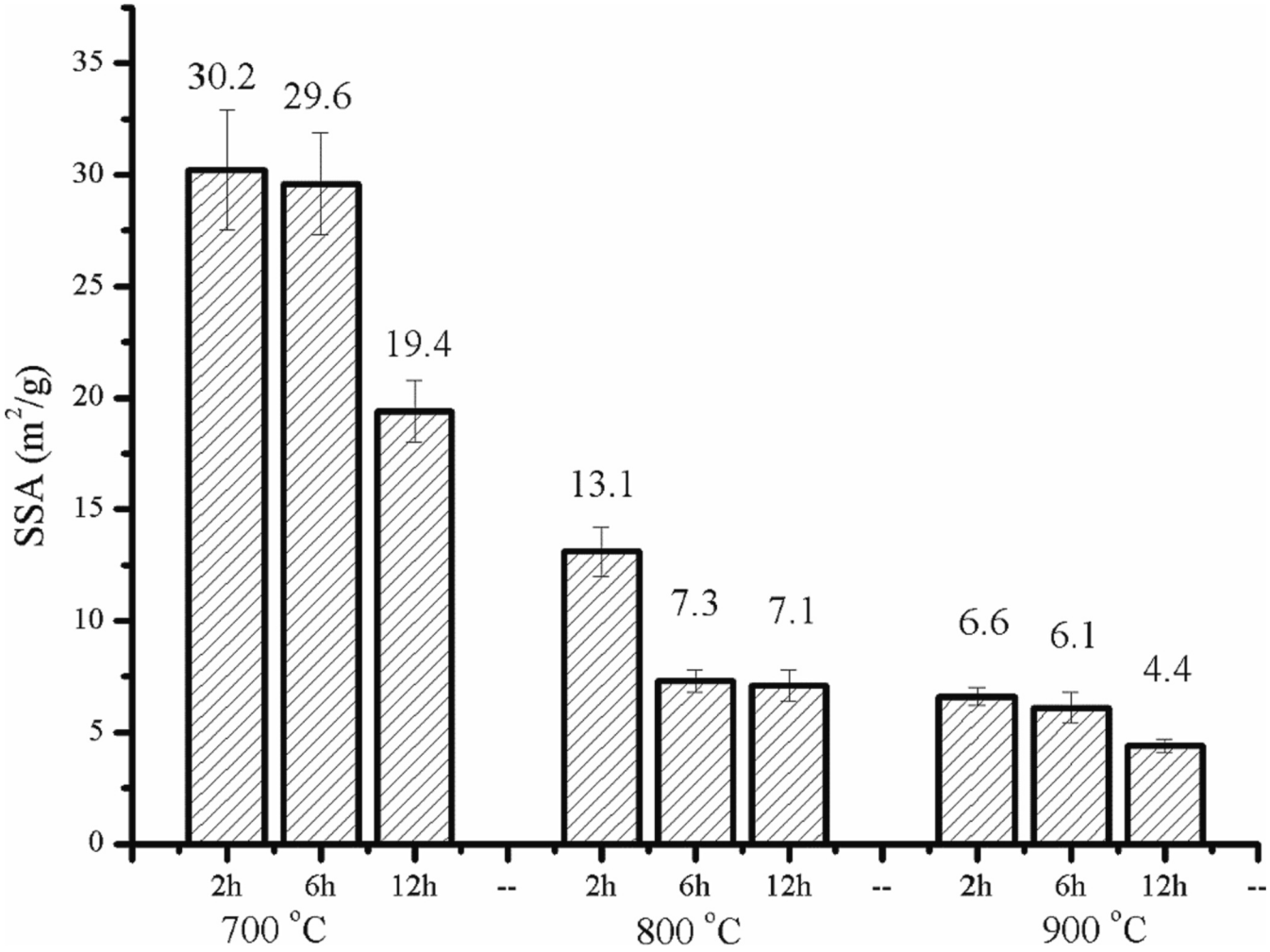

Fig. 4. SSA of MgO obtained from calcination of synthesized $MgC_2O_4{\cdot}2H_2O$ (from reject brine) under different calcination temperature and duration.

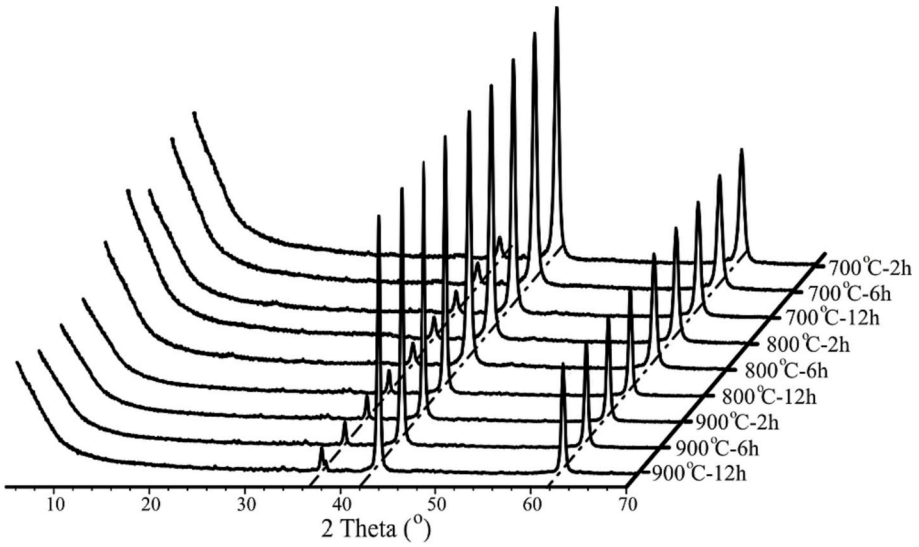

Fig. 5. XRD diffractograms of MgO obtained from calcination of synthesized $MgC_2O_4{\cdot}2H_2O$ (from reject brine) under different calcination temperatures and durations.

exhibited a higher SSA than 13 (out of the 21) commercial products. Extensive studies have revealed the positive correlation between SSA and reactivity, which indicated the higher reactivity of the synthesized MgO comparing to the 13 commercial MgO products [10,42,43]. With different values of SSA, the application scenarios of MgO can vary. Generally, the SSA of MgO used as a cementitious binder reported in

Table 5
Crystallite size, primary particle size and pore volume of MgO samples.

Calcination temperature (°C)	700			800			900		
Calcination duration (h)	2	6	12	2	6	12	2	6	12
G_{XRD} (nm)	14.3	15.6	17.8	18.1	18.1	20.2	21.7	26.3	28.1
SSA (m^2/g)	30.2 ± 2.7	29.6 ± 2.3	19.4 ± 1.4	13.1 ± 1.1	7.3 ± 0.5	7.1 ± 0.7	6.6 ± 0.4	6.1 ± 0.7	4.4 ± 0.3
G_{BET} (nm)	52.3	62.3	115.1	115.1	146.4	173.9	123.6	137.9	157.5
G_{BET}/G_{XRD}	3.9	3.6	4.8	7.0	12.6	11.6	11.6	10.4	13.5
Pore volume (cm^3/g)	0.175 ± 0.016	0.145 ± 0.012	0.109 ± 0.007	0.086 ± 0.005	0.029 ± 0.002	0.028 ± 0.002	0.024 ± 0.003	0.023 ± 0.002	0.023 ± 0.003

Table 6
Comparison of SSA, G_{BET}, G_{XRD} and AR of the obtained MgO with commercial reactive MgO.

Rank	Symbol	Source	SSA (m^2/g)	G_{BET} (nm)	G_{XRD} (nm)	AR = G_{BET}/G_{XRD}
1	DSP	Dead Sea Periclase, Israel	144.93	11.52	11.1	1
2	IM	Intermag Ltd., UK	118.26	14.11	12.3	1.2
3	N50	Richard Baker Harrison Ltd., China	110.82	15.06	14.7	1
4	CNSH-99	SYCC,CN	86.945	19.2	11.8	1.6
5	Unimag	Premier Chemicals, USA	79.9	20.89	–	–
6	XLM	Causmag, Australia	75.2	22.19	16.4	1.4
7	–	83CR (Richard Baker Harrison Ltd., Greece)	47.8	34.92	22.7	1.5
8	CNSH-85	SYCC,CN	33.451	49.9	25.3	2
9	**Reactive MgO obtained in this study**		**30.2**	**52.3**	**14.3**	**3.9**
10	K10	Styromag, Australia	29.13	57.29	22.6	2.5
11	NOR	Richard Baker Harrison Ltd., Greece	24.3	68.68	36.8	1.9
12	83CGb	Richard Baker Harrison Ltd., Greece	20.3	82.22	30.9	2.7
13	UKNK-92	RBH,UK	19.776	84.4	27.4	3.1
14	AU-97	IS,SG	17.098	97.6	33.7	2.9
15	94/325	Richard Baker Harrison Ltd., China	16.31	102.33	43	2.4
16	83CS	Richard Baker Harrison Ltd., Greece	15	82.22	30.9	2.7
17	UKCN-90	RBH,UK	13.437	124.2	37.2	3.3
18	AU-90	ISS,SG	11.311	147.6	32.3	4.6
19	CNSD-92	LCTM,CN	11.058	150.9	34.4	4.4
20	CNLN-92	LCTM,CN	5.754	290.1	40.4	7.2
21	CNSD-99	SYCC,CN	4.404	379	29.7	12.7
22	94/200	Richard Baker Harrison Ltd., China	4.37	381.92	53	7.2

literature covered a wide range from 0.6 to 75.2 m^2/g, including the use of MgO as a sole binder, a partial replacement of PC, or as a stabilizer of wastes and soils [44–49] Earlier studies [41] reported that higher reactivity led to improved hydration, which could facilitate the strength development of the matrix. Furthermore, the positive correlation between AR and strength of RMC-based concrete was also revealed. The AR of MgO obtained in this study was higher than 15 of the commercial counterparts, demonstrating its potential use as a low-carbon binder system. Apart from its use in construction, the high SSA of MgO obtained in this study allows its potential use for adsorption applications, such as removing impurities and pollutants from liquids and gases due to the high surface absorbent performance [50]. Previous research on the use of MgO in wastewater treatment demonstrated that higher SSA led to increased removal of boron and fluorine [51]. Overall, this comparison with commercial MgO products indicated the compatibility of the obtained MgO with those available on the market.

To enable to the wider application of MgO synthesized in this study, including high-end use in the pharmaceutical, agricultural, chemical and refractory industries, where the SSA requirement is usually >100 m^2/g [14,52–56], the SSA and other characteristics (e.g. reactivity and purity) of the MgO produced through this route could be further enhanced through (1) adjusting some key parameters such as the precipitation reaction temperature, pH, and suspension aging time of $Mg(OH)_2$; (2) optimizing calcination conditions such as temperature and duration; and (3) further milling the obtained MgO particles [57–59].

4. Conclusions

This study demonstrated the successful synthesis of high-purity reactive MgO from reject brine through a controlled pH selective precipitation process. By introducing oxalic acid ($H_2C_2O_4{\cdot}2H_2O$) into the reject brine, the precise separation of Ca^{2+} and Mg^{2+} ions was achieved, leading to the formation of $CaC_2O_4{\cdot}H_2O$ and $MgC_2O_4{\cdot}2H_2O$. Subsequent calcination of the optimized $MgC_2O_4{\cdot}2H_2O$ yielded reactive MgO with an enhanced purity and yield. The investigation included the evaluation of the key parameters that influenced the synthesis. This involved a comparison of the yield and purity of $MgC_2O_4{\cdot}2H_2O$ and reactive MgO, and a comprehensive characterization of the chemical and physical properties of the resulting MgO. A correlation between the calcination conditions such as temperature and duration, and the properties of resulting MgO was established.

In the first step, the results revealed that a Ca^{2+}:$H_2C_2O_4{\cdot}2H_2O$ ratio of 1:2, Mg^{2+}:$H_2C_2O_4{\cdot}2H_2O$ ratio of 1:1.5 and a pH of 3 was the optimum condition, resulting in the synthesis of $MgC_2O_4{\cdot}2H_2O$ with an ultra-high purity of 99.6 % and a high Mg^{2+} recovery of 94.1 %. This was followed by the second step, during which the synthesized $MgC_2O_4{\cdot}2H_2O$ was then calcined at specific temperatures and durations. The influence of the calcination conditions on the reactivity of the resulting MgO was studied and the key parameters were revealed. A reduction in the SSA of MgO with an increase in the calcination temperature and duration was observed. Among the conditions investigated, the calcination of $MgC_2O_4{\cdot}2H_2O$ at 700 °C for 2 h generated the most reactive MgO with a SSA of 30.2 m^2/g, which was higher than 13 (out of 21) commercial reactive MgO powders available in the market. The results indicated that the quality of MgO obtained in this study could meet the standards of commercial counterparts and be potentially used in high-end applications other than the cement industry. In future studies, the potential use of other organic acids for the precipitation of Ca and Mg components and recovery of other metals from different brine sources can be further

investigated.

CRediT authorship contribution statement

Haoliang Dong: Conceptualization, Methodology, Formal analysis, Writing – original draft. **Xi Xiao:** Conceptualization, Methodology, Formal analysis, Writing – original draft. **En-Hua Yang:** Conceptualization, Methodology, Writing – review & editing, Supervision. **Cise Unluer:** Conceptualization, Methodology, Writing – review & editing, Supervision.

Declaration of competing interest

None.

Data availability

No data was used for the research described in the article.

Acknowledgement

This study was conducted via financial support from the Ministry of National Development, Singapore (CoT-V1-2020-1). Cise Unluer received financial support from The Royal Society (project ref.: ICA\R1 \201310).

References

[1] S.O. Gardarsdottir, E. De Lena, M. Romano, S. Roussanaly, M. Voldsund, J.-F. Pérez-Calvo, D. Berstad, C. Fu, R. Anantharaman, D. Sutter, Comparison of technologies for CO2 capture from cement production—part 2: cost analysis, Energies 12 (2019) 542.
[2] USGS, Mineral commodity summaries 2023, in: National Minerals Information Center, U.S. Geological Survey, 2023.
[3] V. Sousa, J.A. Bogas, Comparison of energy consumption and carbon emissions from clinker and recycled cement production, J. Clean. Prod. 306 (2021), 127277.
[4] A. Cantini, L. Leoni, F. De Carlo, M. Salvio, C. Martini, F. Martini, Technological energy efficiency improvements in cement industries, Sustainability 13 (2021) 3810.
[5] N. Mohamad, K. Muthusamy, R. Embong, A. Kusbiantoro, M.H. Hashim, Environmental impact of cement production and solutions: a review, Mater. Today Proc. 48 (2022) 741–746.
[6] C. Unluer, A. Al-Tabbaa, Enhancing the carbonation of MgO cement porous blocks through improved curing conditions, Cem. Concr. Res. 59 (2014) 55–65.
[7] S. Ruan, C. Unluer, Influence of supplementary cementitious materials on the performance and environmental impacts of reactive magnesia cement concrete, J. Clean. Prod. 159 (2017) 62–73.
[8] S. Ruan, C. Unluer, Comparison of the environmental impacts of reactive magnesia and calcined dolomite and their performance under different curing conditions, J. Mater. Civ. Eng. 30 (2018), 04018279.
[9] N. Dung, C. Unluer, Carbonated MgO concrete with improved performance: the influence of temperature and hydration agent on hydration, carbonation and strength gain, Cem. Concr. Compos. 82 (2017) 152–164.
[10] H. Dong, C. Unluer, E.-H. Yang, A. Al-Tabbaa, Recovery of reactive MgO from reject brine via the addition of NaOH, Desalination 429 (2018) 88–95.
[11] I. Singh, R. Hay, K. Celik, Recovery and direct carbonation of brucite from desalination reject brine for use as a construction material, Cem. Concr. Res. 152 (2022), 106673.
[12] H. Dong, C. Unluer, E.-H. Yang, A. Al-Tabbaa, Synthesis of reactive MgO from reject brine via the addition of NH4OH, Hydrometallurgy 169 (2017) 165–172.
[13] S. Ruan, E.-H. Yang, C. Unluer, Production of reactive magnesia from desalination reject brine and its use as a binder, J. CO2 Util. 44 (2021), 101383.
[14] A.A. Pilarska, Ł. Klapiszewski, T. Jesionowski, Recent developments in the synthesis, modification and application of Mg (OH) 2 and MgO: a review, Powder Technol. 319 (2017) 373–407.
[15] M. Chinthala, A. Balakrishnan, P. Venkataraman, V. Manaswini Gowtham, R. K. Polagani, Synthesis and applications of nano-MgO and composites for medicine, energy, and environmental remediation: a review, Environ. Chem. Lett. 19 (2021) 4415–4454.
[16] C. Unluer, Carbon dioxide sequestration in magnesium-based binders, in: Carbon Dioxide Sequestration in Cementitious Construction Materials, Elsevier, 2018, pp. 129–173.
[17] M.H. El-Naas, Reject Brine Management, Desalination, Trends and Technologies, 2011, pp. 237–252.
[18] A.M.O. Mohamed, M. Maraqa, J. Al Handhaly, Impact of land disposal of reject brine from desalination plants on soil and groundwater, Desalination 182 (2005) 411–433.
[19] M.K.K. Nassar, R.M. El-Damak, A.H.M. Ghanem, Impact of desalination plants brine injection wells on coastal aquifers, Environ. Geol. 54 (2007) 445–454.
[20] E. Jones, M. Qadir, M.T. van Vliet, V. Smakhtin, S.-m. Kang, The state of desalination and brine production: a global outlook, Sci. Total Environ. 657 (2019) 1343–1356.
[21] F. Vassallo, D. La Corte, N. Cancilla, A. Tamburini, M. Bevacqua, A. Cipollina, G. Micale, A pilot-plant for the selective recovery of magnesium and calcium from waste brines, Desalination 517 (2021), 115231.
[22] V. Vallès, M.F. de Labastida, J. López, G. Battaglia, D. Winter, S. Randazzo, A. Cipollina, J. Cortina, Sustainable recovery of critical elements from seawater saltworks bitterns by integration of high selective sorbents and reactive precipitation and crystallisation: developing the probe of concept with on-site produced chemicals and energy, Sep. Purif. Technol. 306 (2023), 122622.
[23] InnovationNewsNetwork, New method to extract magnesium from seawater, in: Energy, https://www.innovationnewsnetwork.com/new-method-extract-magnesium-from-seawater/25685/, 2022. https://www.innovationnewsnetwork.com/new-method-extract-magnesium-from-seawater/25685/.
[24] Q. Wang, E. Nakouzi, E.A. Ryan, C.V. Subban, Flow-assisted selective mineral extraction from seawater, Environ. Sci. Technol. Lett. 9 (2022) 645–649.
[25] J. Liao, Q. Chen, N. Pan, X. Yu, X. Gao, J. Shen, C. Gao, Amphoteric blend ion-exchange membranes for separating monovalent and bivalent anions in electrodialysis, Sep. Purif. Technol. 242 (2020), 116793.
[26] P. Loganathan, G. Naidu, S. Vigneswaran, Mining valuable minerals from seawater: a critical review, Environ. Sci. Water Res. Technol. 3 (2017) 37–53.
[27] H. Dong, C. Unluer, E.H. Yang, A. Al-Tabbaa, Synthesis of reactive MgO from reject brine via the addition of NH_4OH, Hydrometallurgy 169 (2017) 165–172.
[28] K.T. Tran, T. Van Luong, J.W. An, D.J. Kang, M.J. Kim, T. Tran, Recovery of magnesium from Uyuni salar brine as high purity magnesium oxalate, Hydrometallurgy 138 (2013) 93–99.
[29] T. Holth, Separation of calcium from magnesium by oxalate method, Anal. Chem. 21 (1949) 1221–1226.
[30] P.J. Elving, E.R. Caley, Separation of magnesium as oxalate, Ind. Eng. Chem. Anal. Ed. 9 (1937) 558–562.
[31] A.L. Patterson, The Scherrer formula for X-ray particle size determination, Phys. Rev. 56 (1939) 978–982.
[32] K. Itatani, M. Nomura, A. Kishioka, M. Kinoshita, Sinterability of various high-purity magnesium-oxide powders, J. Mater. Sci. 21 (1986) 1429–1435.
[33] M. Orlando, L. Kuplich, D. De Souza, H. Belich, J. Depianti, C. Orlando, E. Medeiros, P. Da Cruz, L. Martinez, H. Corrêa, Study of calcium oxalate monohydrate of kidney stones by X-ray diffraction, Powder Diffract. 23 (2008) S59–S64.
[34] W.R. Eubank, Calcination studies of magnesium oxides, J. Am. Ceram. Soc. 34 (1951) 225–229.
[35] K. Itatani, K. Koizumi, F.S. Howell, A. Kishioka, M. Kinoshita, Agglomeration of magnesium oxide particles formed by the decomposition of magnesium hydroxide. 1. Agglomeration at increasing temperature, J. Mater. Sci. 23 (1988) 3405–3412.
[36] E. Alvarado, L.M. Torres-Martinez, A.F. Fuentes, P. Quintana, Preparation and characterization of MgO powders obtained from different magnesium salts and the mineral dolomite, Polyhedron 19 (2000) 2345–2351.
[37] L.W. Mo, M. Deng, M.S. Tang, Effects of calcination condition on expansion property of MgO-type expansive agent used in cement-based materials, Cem. Concr. Res. 40 (2010) 437–446.
[38] J.K. Bartley, C. Xu, R. Lloyd, D.I. Enache, D.W. Knight, G.J. Hutchings, Simple method to synthesize high surface area magnesium oxide and its use as a heterogeneous base catalyst, Appl. Catal. B Environ. 128 (2012) 31–38.
[39] F. Jin, A. Al-Tabbaa, Characterisation of different commercial reactive magnesia, Adv. Cem. Res. 26 (2014) 101–113.
[40] K. Itatani, A. Itoh, F.S. Howell, A. Kishioka, M. Kinoshita, Densification and microstructure development during the sintering of submicrometer magnesium-oxide particles prepared by a vapor-phase oxidation process, J. Mater. Sci. 28 (1993) 719–728.
[41] T. Mi, E.-H. Yang, C. Unluer, Investigation of the properties of reactive MgO-based cements and their effect on performance, Cem. Concr. Compos. 138 (2023), 104984.
[42] H. Dong, E.-H. Yang, C. Unluer, F. Jin, A. Al-Tabbaa, Investigation of the properties of MgO recovered from reject brine obtained from desalination plants, J. Clean. Prod. 196 (2018) 100–108.
[43] S.H. Chu, E.H. Yang, C. Unluer, Chemical synthesis of magnesium oxide (MgO) from brine towards minimal energy consumption, Desalination 556 (2023), 116594.
[44] Y. Song, X. Qian, D. Yan, C. Unluer, Y. Peng, D. Kong, C. Hu, S. Wang, S. Ruan, Understanding the role of seeds in reactive magnesia cement (RMC) formulations, J. Am. Ceram. Soc. 106 (2023) 3812–3831.
[45] R. Hay, B. Peng, K. Celik, Filler effects of CaCO3 polymorphs derived from limestone and seashell on hydration and carbonation of reactive magnesium oxide (MgO) cement (RMC), Cem. Concr. Res. 164 (2023), 107040.
[46] L. Mo, D.K. Panesar, Effects of accelerated carbonation on the microstructure of Portland cement pastes containing reactive MgO, Cem. Concr. Res. 42 (2012) 769–777.
[47] D.-L. Wang, C.-S. Tang, X.-H. Pan, R. Wang, J.-W. Li, Z.-H. Dong, B. Shi, Construction and demolition waste stabilization through a bio-carbonation of reactive magnesia cement for underwater engineering, Constr. Build. Mater. 335 (2022), 127458.
[48] L. Vandeperre, M. Liska, A. Al-Tabbaa, Microstructures of reactive magnesia cement blends, Cem. Concr. Compos. 30 (2008) 706–714.

[49] R. Hay, N. Dung, A. Lesimple, C. Unluer, K. Celik, Mechanical and microstructural changes in reactive magnesium oxide cement-based concrete mixes subjected to high temperatures, Cem. Concr. Compos. 118 (2021), 103955.
[50] J. Hu, Z. Song, L. Chen, H. Yang, J. Li, R. Richards, Adsorption properties of MgO (111) nanoplates for the dye pollutants from wastewater, J. Chem. Eng. Data 55 (2010) 3742–3748.
[51] T. Kameda, Y. Yamamoto, S. Kumagai, T. Yoshioka, Effect of the specific surface area of MgO on the treatment of boron and fluorine, Appl Water Sci 10 (2020) 104.
[52] M.A. Shand, The Chemistry and Technology of Magnesia, 2006.
[53] E.K. Lee, K.D. Jung, O.S. Joo, Y.G. Shul, Magnesium oxide as an effective catalyst in catalytic wet oxidation of H2S to sulfur, React. Kinet. Catal. Lett. 82 (2004) 241–246.
[54] M.A. Caraballo, T.S. Rotting, F. Macias, J.M. Nieto, C. Ayora, Field multi-step limestone and MgO passive system to treat acid mine drainage with high metal concentrations, Appl. Geochem. 24 (2009) 2301–2311.
[55] G. Moussavi, M. Mahmoudi, Removal of azo and anthraquinone reactive dyes from industrial wastewaters using MgO nanoparticles, J. Hazard. Mater. 168 (2009) 806–812.
[56] F. Wang, F. Jin, Z.T. Shen, A. Al-Tabbaa, Three-year performance of in-situ mass stabilised contaminated site soils using MgO-bearing binders, J. Hazard. Mater. 318 (2016) 302–307.
[57] L. Huang, Z. Yang, S. Wang, Influence of calcination temperature on the structure and hydration of MgO, Constr. Build. Mater. 262 (2020), 120776.
[58] S. Yousefi, B. Ghasemi, M. Tajally, A. Asghari, Optical properties of MgO and Mg (OH) 2 nanostructures synthesized by a chemical precipitation method using impure brine, J. Alloys Compd. 711 (2017) 521–529.
[59] A. Khalil, K. Celik, Optimizing reactivity of light-burned magnesia through mechanical milling, Ceram. Int. 45 (2019) 22821–22828.